https://doi.org/10.5194/amt-2019-391
Preprint. Discussion started: 5 November 2019

Atmospheric Measurement Techniques Discussions

Instrumental characteristics and Greenhouse gases measurement capabilities of the Compact High-spectral Resolution Infrared Spectrometer: CHRIS.

Marie-Thérèse El Kattar[1], **Frédérique Auriol**[1], **and Hervé Herbin**[1]

[1]Univ. Lille, CNRS, UMR 8518 - LOA - Laboratoire d'Optique Atmosphérique, F-59000 Lille, France

Correspondence to: Hervé Herbin
(herve.herbin@univ-lille.fr)

https://doi.org/10.5194/amt-2019-391
Preprint. Discussion started: 5 November 2019

Atmospheric Measurement Techniques Discussions

Abstract. Ground-based high spectral resolution infrared measurements are an efficient way to obtain accurate tropospheric abundances of different gaseous species and in particular GreenHouse Gases (GHG), such as CO_2 and CH_4. Many ground-based spectrometers are used in the NDACC and TCCON networks to validate the Level 2 satellite data, but their large dimensions and heavy mass makes them inadequate for field campaigns. To overcome these problems, the use of portable spectrometers was recently investigated. In this context, this paper deals with the CHRIS (Compact High-spectral Resolution Infrared Spectrometer) prototype with unique characteristics such as its high spectral resolution (0.135 cm^{-1} non-apodized) and its wide spectral range (680 to 5200 cm^{-1}). Its main objective is the characterization of gases and aerosols in the infrared thermal region, that's why it requires high radiometric precision and accuracy, which is achieved by performing spectral and radiometric calibrations that will be presented in this paper. Also, CHRIS's capabilities to retrieve CO_2 and CH_4 vertical profiles are presented through a complete information content analysis, a channel selection and an error budget estimation in the attempt to join the ongoing campaigns, such as MAGIC, to monitor the GHG and validate the actual and future space missions.

1 Introduction

Remote sensing techniques have gained a lot of popularity in the past few decades due to the increasing need of a continuous monitoring of the atmosphere (Persky (1995)). Greenhouse gases, trace gases but also clouds and aerosols are detected and retrieved, thus improving our understanding of the dynamics of the atmosphere. Global scale observations are achieved using satellites, and one major technique is the InfraRed High Spectral Resolution (IRHSR). This technique offers radiometrically precise observations at high spectral resolution (Revercomb et al. (1988)), where quality measurements of absorption spectra are obtained. TANSO-FTS (Suto et al. (2006)), IASI (Clerbaux et al. (2007)) and AIRS (Aumann et al. (2003)) are examples of satellite sounders covering the Thermal InfraRed (TIR) region. The observations acquired from such satellites have many advantages such as: day and night data acquisition, possibility to measure concentrations of different gases, the ability to cover the land and sea surfaces (Herbin et al. (2013a)), and the advantage of being highly sensitive to aerosols types (Clarisse et al. (2010)). These spectrometers also have some disadvantages: local observations are challenging to achieve due to the pixel size that limits the spatial resolution, and the sensitivity in the low atmospheric layers is weak, where many short-lived gaseous species are emitted but rarely detected.

To fill these gaps, ground-based instruments are used as a complementary technique and one famous high-precision Fourier transform spectrometer is the IFS125HR from Bruker™, which will be briefly discussed in Section (3.5), further details can be found in Wunch et al. (2011). Twenty instruments are currently deployed all over the world in two major international networks: TCCON (https://tccondata.org/) and NDACC (https://www.ndsc.ncep.noaa.gov/). This particular instrument has a very large size (1x1x3 m) and a mass well beyond a hundred kilograms, and therefore achieving a long optical path difference leading to a very high spectral resolution (5x10$^{-3}cm^{-1}$). Despite its outstanding capabilities, this spectrometer is not suitable for field campaigns so it is mainly used to validate the Level 2 satellite data, thus limiting the scientifically important ground-based extension of atmospheric measurement on a global scale.

One alternative is the new IFS125M from Bruker (Pathatoki et al. (2019)) which is the mobile version of the well-established IFS125HR spectrometer. This spectrometer provides the highest resolution available for a commercial mobile FTIR spectrometer but it still has a length of about 2 m and requires on-site realignment by qualified personnel. Another alternative is the use of several compact medium-to-low resolution instruments that are currently under investigation such as a grating spectrometer (0.16 cm^{-1}), a fiber Fabry-Perot interferometer (both setups presented in Kobayashi et al. (2010)) and the IFS66 from Bruker (0.11 cm^{-1}) described in Petri et al. (2012). The EM27-SUN is the first instrument that offered a compact optically stable, high Signal-to-noise ratio, transportable spectrometer (Gisi et al. (2012)) that operates in the SWIR (Short Wavelength InfraRed) region. A new prototype called CHRIS (Compact High spectral Resolution Infrared Spectrometer) was conceived to satisfy some very specific characteristics: high spectral resolution (0.135 cm^{-1}, better than TANSO-FTS and the future IASI-NG); a large spectral band (680-5200 cm^{-1}) to cover the current and future satellite range and optimize the quantity of the measured species that will allow us the validation of the satellite data. Furthermore, this prototype had to be transportable and could operate for several hours on battery so it will be suitable for field campaigns. The full presentation of the characteristics and the calibration of this instrumental prototype will be presented in Section 2.

Since carbon dioxide (CO_2) and methane (CH_4) are the two main greenhouse gases emitted by human activities, multiple campaigns have been put in place like the MAGIC (Monitoring of Atmospheric composition and Greenhouse gases through multi-Instruments Campaigns) initiative, to better understand the vertical exchange of these GHG along the atmospheric column and to contribute to the preparation and validation of future space missions dedicated to monitor GHG. CHRIS is part of this ongoing mission and this work will demonstrate for the first time the capabilities of such a setup in achieving GHG

https://doi.org/10.5194/amt-2019-391
Preprint. Discussion started: 5 November 2019

Atmospheric Measurement Techniques Discussions

measurements, where the forward model, state vector and error analysis will be explained in Section 3.
In this context, we present in Section 3.5, a complete information content study for the retrieval of CO_2 and CH_4 of two other ground-based instruments that also participated in the MAGIC campaign: a comparison study with the IFS125HR instrument; and since CHRIS and EM27-SUN have a common band in the SWIR region, a study to investigate the spectral synergy in order to quantify the complementary aspects of the TIR/SWIR coupling for these two instruments. Moreover, Section 4 describes the channel selection made in this study. Finally, we will summarize our results and present perspectives for future applications; in particular, the inversion of GHG.

2 The CHRIS spectrometer

CHRIS is an instrumental prototype built by Bruker™and used in different domains of atmospheric optics where its recorded spectra contains signatures of various atmospheric constituents such as gases (H_2O, CO_2, CH_4), and other particular species. The capacity to measure these species from a technical point of view as well as the characterization of this prototype in terms of spectral and radiometric calibrations will be presented in the following sections.

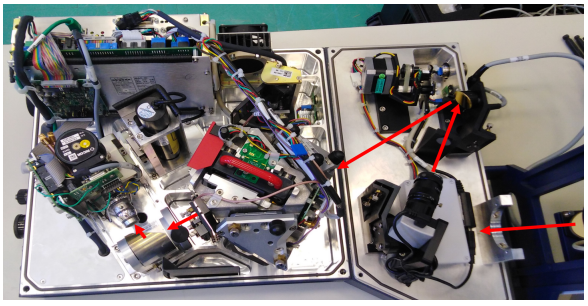

Fig. 1: An internal look of CHRIS, the red arrows illustrates the optical path of the solar beam inside the spectrometer.

2.1 General characteristics

CHRIS is a portable instrumental prototype with a mass of approximately 40 kgs and dimensions of 70x40x40 cm which makes it easy to operate on the field. The tracker, similar to the one installed on the EM27-SUN and described in details in Gisi et al. (2012), leads the solar radiation through multiple reflections on the mirrors to a wedged fused silica window.
An internal look of CHRIS is shown in Fig. 1, where the optical path of the solar beam is represented with red arrows: after multiple reflections on the tracker's mirrors, the solar radiation enters the spectrometer through the opening and is then reflected by the first mirror where the CCD camera verifies the collimation of the beam on the second mirror having the solar filter. At this level, CHRIS have a filter wheel that can be equipped with up to 5 optical filters with a diameter of 25mm. Filters are widely used when making solar measurements to reduce noise and non-linearity effects. After reflection on the second mirror, the beam enters the rock solid Michelson interferometer which has two cube-corner mirrors to ensure the optical alignment stability of the beam and a KBr beamsplitter. After that, the radiation is blocked by an adjustable aperture stop which can be set between 1 and 18 mm. This limits the parallel beam parameter, and can be used to reduce the intensity of the incoming sunlight in case of saturation of the detector. The remaining radiation falls on the MCT detector, then it is digitized to obtain the solar absorption spectra. This detector is known for its non-linearity and uses a closed-cycle stirling cooling system (a.k.a. cryo-cooler) so no liquid nitrogen has to be used. As the vibrations of the compressor may introduce noise in the spectra, a high scanning velocity (120 KHz) is used.
A standard non-stabilized He-Ne laser controls the sampling of the interferogram. The condensation of the warm humid air on the beamsplitter due to its transportation between cold and warm environments, is the main reason of the use of a dessicant cartridge, so the spectrometer can operate in various environmental conditions. CHRIS has also an internal blackbody, which can be heated up to 353 K to make that sure that there is no potential drift in the TIR region, and it also serves as an optical source to verify regularly the response of the detector.

https://doi.org/10.5194/amt-2019-391
Preprint. Discussion started: 5 November 2019

Atmospheric Measurement Techniques Discussions

2.2 Measurements and analysis

CHRIS has a Maximum Optical Path Difference (MOPD) of 4.42 cm resulting in a non-apodized spectral resolution of 0.135 cm^{-1} with a spectral sampling every 0.06025 cm^{-1} to satisfy the Nyquist criterion. Each spectrum corresponds to the solar transmission light in the total atmospheric column in a Field Of View (FOV) of 0.006 mrad. The spectral range spans the region from 680 to 5200 cm^{-1} (1.9 to 14.7 µm) which corresponds to the Middle InfraRed region (MIR). The Signal-to-Noise Ratio (SNR) is an estimation of the root mean squared noise of the covered spectral domain and can be calculated in OPUS (the running program for CHRIS) using the function SNR with option fit parabola; it is estimated to be approximately 780. These instrumental qualities, summarized in Table 2, will enable this prototype not only to measure CO_2 and CH_4, but also to detect other trace gases with weak absorption.

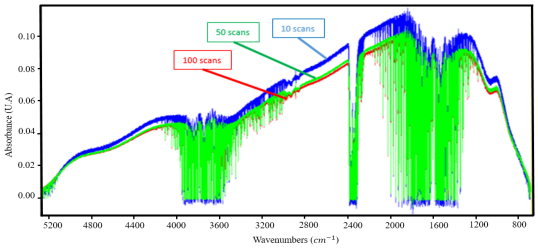

Fig. 2: Representation of 3 spectra with 3 different scan number.

2.2.1 Technical study

A technical study was conducted on this prototype in order to evaluate its capabilities. One of the most important findings is the effect of the number of scan on the measured spectra. In practice, a scan is the acquisition of a single interferogram when the mobile mirror of the Michelson interferometer begins data collection at the Zero Path Difference (ZPD) and finishes at the maximum length, therefore achieving the highest resolution required. In Fig.2, the spectrum with 10 scans has a higher amplitude than that of 50 and 100 scans. On the other hand, if we look closely, the spectra of 50 and 100 scans are clearly less noisy than that of the 10 scans. This is due to the fact that the increase in the number of scans causes an increase in the SNR which leads to the decrease of the noise. However, there is a limit to the number of scans beyond which no improvement of the SNR is obtained. The SNR is proportional to the square root of the acquisition time (number of scans), also known as the Fellgett's advantage and since the detector is shot noise dominated, the improvement of the SNR with the number of scans is blocked at a certain value, and this is why the spectra of 50 and 100 scans do not have a big difference. An optimized criteria is chosen to select the appropriate number of scans: when the wanted species has a fast changing concentration, such as volcanic plumes, a relatively small number of scans is needed to be able to follow temporally the change in the atmospheric composition; while in contrast, when measurements of relatively stable atmospheric composition are made, for example GHG (CO_2 and CH_4), the number of scans can be increased to 100.
Another important feature is the effect of the gain amplitude (and pre-amplifiers) on the spectra, which plays the role of amplifying the signal before digitization. Those parameters should be chosen in a way that the numeric count, falls in a region where no detector saturation occurs. If the gain is increased of a certain amount, the background noise is increased by the same amount. The use of such an option in the measurement procedure might be considered in cases where the signal is very weak, like the lunar measurements. Note that there are other ways to increase the intensity of the signal like using signal amplifying filters (see Section 2.1), or increasing the aperture stop diameter.

2.2.2 Measurement

CHRIS's method of data acquisition is explained as follows: the interferograms are sampled and digitized by an Analogue-to-Digital Converter (ADC), and then numerically resampled at constant intervals of OPD by a He-Ne reference laser signal controlled by the aperture stop diameter. In order to determine a suitable compromise between the latter and to avoid the saturation of the signal, measurements must be done in a clear (no clouds or aerosols) and non-polluted (no gases with high chemical reaction) atmosphere. For this purpose, a field campaign was carried out at the "El Observatorio Atmosférico de Izaña" (28.30°N, 16.48°W) in the Tenerife island. This particular observatory site is high in altitude (2374 m), away from

https://doi.org/10.5194/amt-2019-391
Preprint. Discussion started: 5 November 2019

Atmospheric Measurement Techniques Discussions

pollution sites and has an IFS125HR listed in both the NDACC and TCCON networks. Saturation of the CHRIS's detector is reached at a value of 32000 ADC. The MCT detector is known for its high photometric accuracy but it also exhibits a non-linear response with regard to the energy flux in cases of high incident energy. This led us to choose an aperture stop of 5 mm, which is the best compromise between saturation and incoming energy flux. In the following section, the spectral and radiometric calibrations are discussed in order to convert spectra from numeric counts to radiance expressed in $W.m^{-2}.sr^{-1}.cm$.

An example of the spectra recorded by CHRIS is shown in Fig. 3 where the spectral range spans the region from 680 to 5200 cm^{-1}. The water vapor causes the saturation we see between the bands, thus the 0 signal. Therefore, we divided the spectrum into 4 distinctive spectral bands presented in Table 2: BT (thermal band: 680-1250 cm^{-1}), B1 (1800-2300 cm^{-1}), B2 (2400-3600 cm^{-1}) and B3 (3900-5200 cm^{-1}) and this annotation is used for the rest of the paper.

2.2.3 Spectral and radiometric calibration

The sampling of the interferogram is controlled by a standard, not frequency-stabilized He-Ne laser with a wavelength of 632.8 nm which serves as a reference while converting from the distance scale to the wavenumber scale. This reference wavelength changes in function of the pressure and temperature conditions in which the instrument is placed in, thus the refractive index will change which will lead to an instability in the conversion process and therefore the need for a spectral calibration to reduce this error. To do so, we choose isolated lines in the spectra and apply Eq.1 which is limited by a 0.038 cm^{-1} maximum precision. A Sinc wavefunction is used to re-simulate these absorption lines from the Hitran (Gordon et al. (2017)) database considering non-apodized spectra which allows the exploitation of the full spectral resolution. In short, we choose an intense, non-saturated and always present in the spectra absorption line of H_2O with wavenumber ν, then we compare it with the simulation and calculate its new wavenumber ν^*:

$$\nu^* = \nu(1+\alpha) \tag{1}$$

where α is the calibration factor.

Despite the fact that CHRIS has an internal blackbody, radiometric calibration cannot be overlooked because of its narrow spectral coverage (only the TIR region), and since the radiometric noise, time dependent and wavelength dependent calibration errors are magnified in the inversion process, high radiometric precision is required to derive atmospheric parameters from a spectrum. We calibrate our spectra using the two points calibration method explained in Revercomb et al. (1988). This method consists of using the observations of hot and cold blackbody reference sources which will be used as the basis for the two points calibration at each wavenumber. A cavity blackbody (SR-2 from CI systems) that can be heated up to 1473 K, is used to perform this experiment. These 2 blackbody temperatures are viewed to determine the slope m and offset b (Eq. 2 & 3) which defines the linear instrument response at each wavenumber. The slope and the offset can be written as:

$$m = \frac{S_c - S_h}{B_\nu(T_c) - B_\nu(T_h)} \tag{2}$$

$$b = \frac{S_c * B_\nu(T_h) - S_h * B_\nu(T_c)}{B_\nu(T_h) - B_\nu(T_c)} \tag{3}$$

where S is the blackbody spectrum recorded and B_ν corresponds to the calculated Planck blackbody radiance; the subscripts h and c corresponds respectively to the hot and cold blackbody temperatures. Finally, the calibrated spectrum expressed in radiance is obtained by applying the following formula:

$$L = \frac{S - b}{m} \tag{4}$$

where S is the spectrum recorded by CHRIS. In the retrieval of gases, the spectrometer's line-of-sight (LOS) has to be known for calculating the spectral absorption of the solar radiation while passing through the atmosphere. For this, the time and the duration of each measurement is saved, from which the required effective solar elevation (respectively the Solar Zenith Angle (SZA)) is calculated based on the routine explained in Michalsky (1988).

Moreover, accurate knowledge of the solar radiance in the IR region is required to validate our results since the sun is the initial source of CHRIS. Trishchenko (2006) offered a detailed and extensive study on the matter, and combined the work of four recent solar reference spectra. In our work, two of these reference spectra with 0.1% relative difference are taken into consideration: Kurucz and the American Society of Testing and Materials (ATSM). These solar references agree on one point: the effective brightness temperature depends strongly on the wavenumber. Based on these findings, the Planck function is calculated in each spectral domain of CHRIS, and then adjusted by a polynomial fit. The final calibrated spectrum is shown in Fig. 3. Spectral and radiometric calibrations procedure is automated using a Matlab code to convert the spectra instantly from numeric counts to absolute radiance.

https://doi.org/10.5194/amt-2019-391
Preprint. Discussion started: 5 November 2019

Atmospheric Measurement Techniques Discussions

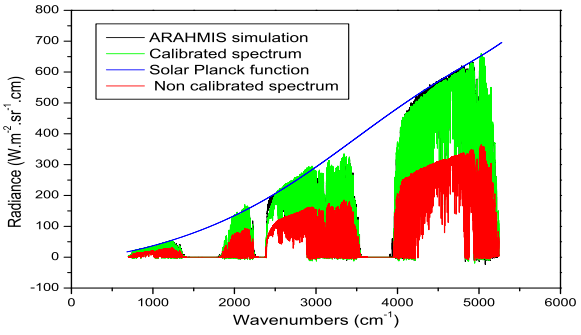

Fig. 3: CHRIS spectrum after calibration. The simulation with ARAHMIS (black) reproduce the calibrated spectrum (green) and fits with the solar Planck function (solid blue line).

3 Information content analysis

The MAGIC campaigns are a french initiative supported by the CNES, that serve as a way of understanding the vertical exchange of the GHG (CO_2 and CH_4) along the atmospheric column through multi-instruments such as satellites, lidar, balloons and ground-based measurements. In this context, CHRIS is one of the instruments used in these campaigns and since it's a prototype, its ability to retrieve these GHG is unknown; hence it is important to perform an information content analysis to quantify the quality of retrieval of these gases.

3.1 The forward model

Accurate calculations of the radiance observed by CHRIS (then divided by the Planck function to obtain the transmittance) are achieved with a line-by-line radiative transfer algorithm ARAHMIS, developed at the Laboratoire d'Optique Atmosphérique (LOA), over the thermal and solar infrared spectral regions (1.9-14.7 µm). Gaseous absorption is calculated with ARAHMIS based on the updated HITRAN 2016 database (Gordon et al. (2017)). The absorption lines are computed assuming a Sinc line shape and no-apodization is applied which allows the exploitation of the full spectral resolution. In this study, the term "all bands" refers to the use of the bands BT, B1, B2 and B3 simultaneously of CHRIS (see Section 2.2.2). Absorption continua (H_2O and CO_2) are also included. The solar pseudo-transmittance spectra reported by Toon (2015) is used as the incident solar spectrum. As mentioned in Section 3.3.2, $Izaña$ offers clear non-polluted measurements since it is high in altitude and away from major pollution sites, so calculations are performed based on the concentration of the desired atmospheric profile with the corresponding profile information including the temperature and humidity.
Figure 4 shows the results of the forward model simulation superimposed with the four infrared bands measured by CHRIS. For each band, we present the influence of the solar spectrum, the GHG in question (CO_2 and CH_4) and the major molecular absorbers in the atmosphere that are not included in our potential inversion process. We can clearly see that with the help of ARAHMIS, CHRIS's signal is very well re-simulated in clear sky conditions.

3.2 Information content theoretical basis

Once the forward model is calculated, we will rely on the formalism of Rodgers (2000) that introduces the optimal estimation theory used for the retrieval, which is widely known elsewhere and summarized here.
In the case of an atmosphere divided in discrete layers, the forward radiative transfer equation gives an analytical relationship between the set of observations y (in this case, the radiance) and the vector of true atmospheric parameters x (i.e. the variables to be retrieved: vertical concentration profile of CO_2 and/or CH_4):

$$y = F(x;b) + \varepsilon, \tag{5}$$

where F is the forward radiative transfer function, b represents the fixed parameters affecting the measurement (e.g. atmospheric temperature, surface emissivity) and ε is the measurement errors vector.
In the following information content study, two matrices: the averaging kernel A and the total error covariance S_x, fully characterize the information provided by CHRIS.

https://doi.org/10.5194/amt-2019-391
Preprint. Discussion started: 5 November 2019

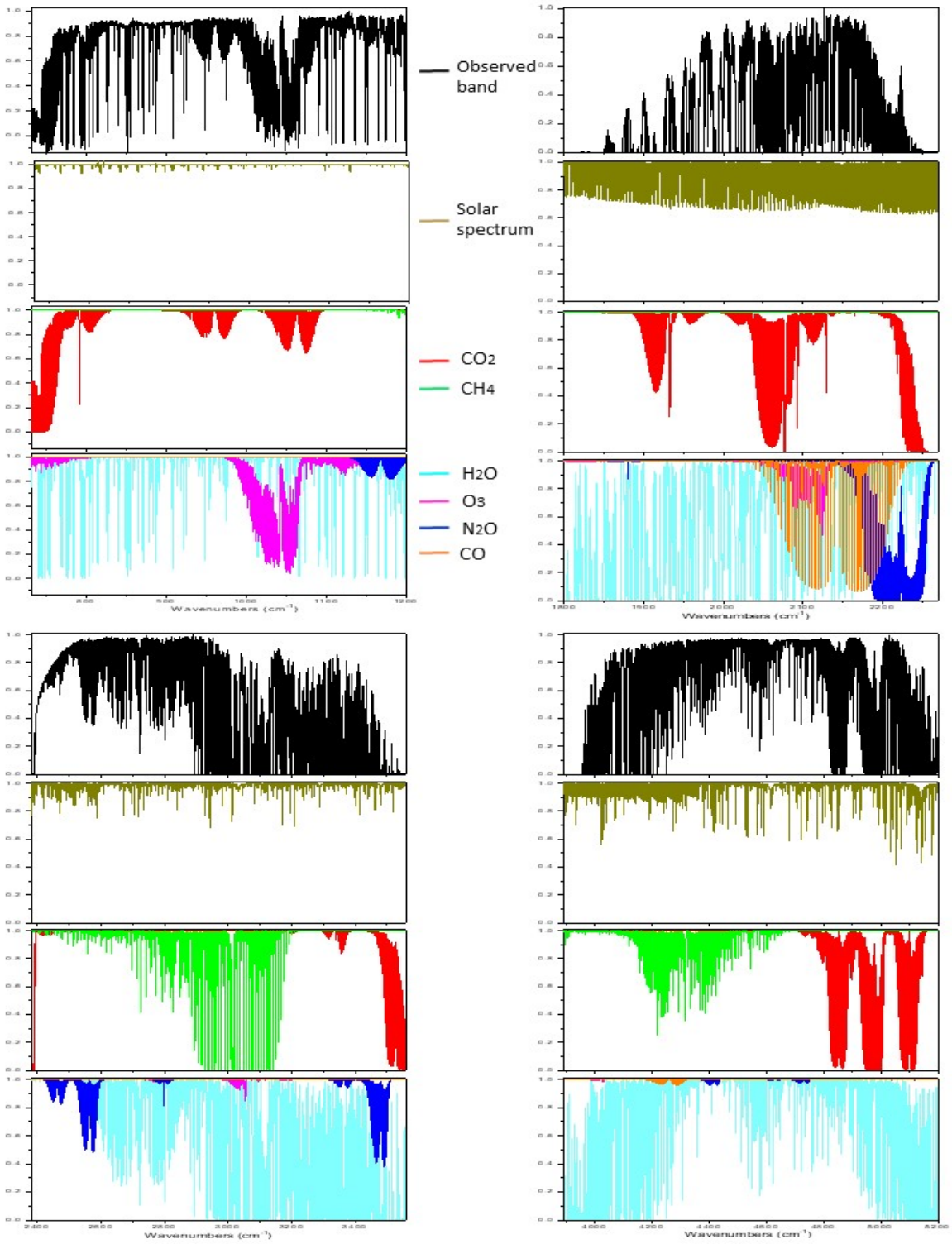

Fig. 4: Measured and simulated CHRIS spectrum in transmittance for clear sky conditions at Izaña observatory. Each band is calculated from the line-by-line forward model ARAHMIS.

https://doi.org/10.5194/amt-2019-391
Preprint. Discussion started: 5 November 2019

Atmospheric Measurement Techniques Discussions

The averaging kernel matrix A, gives a measure of the sensitivity of the retrieved state to the true state, and is defined by:

$$A = \partial\hat{x}/\partial x = GK, \tag{6}$$

where K is the Jacobian matrix (also known as the weighting function), where the ith row is the partial derivatives of the ith measurement with respect to each (j) element of the state vector: $K_{ij} = (\partial F_i/\partial x_j)$, and K^T is its transpose.
The gain matrix G , whose rows are the derivatives of the retrieved state with respect to the spectral points, is defined by:

$$G = \partial\hat{x}/\partial y = (K^T S_\varepsilon K + S_a^{-1})^{-1} K^T S_\varepsilon^{-1}, \tag{7}$$

where S_a is the a priori covariance matrix describing our knowledge of the state space prior to the measurement and S_ϵ represents the forward model and the measured signal error covariance matrix.
At a given level, the peak of the averaging kernel row gives the altitude of maximum sensitivity, whereas its full width at half maximum (FWHM) is an estimate of the vertical resolution. The total Degrees Of Freedom for Signal (DOFS) is the trace of A, which indicates the amount of independent pieces of information that one can extract from the observations with respect to the state vector. A perfect retrieval resulting from an ideal inverse method would lead to an averaging kernel matrix A equal to the identity matrix with a DOFS equal to the size of the state vector. Therefore, each parameter we want to retrieve is attached to the partial degree of freedom represented by each diagonal element of A.
The second important matrix in the IC study is the error covariance matrix S_x, which describes our knowledge of the state space posterior to the measurement. Rodgers (2000) demonstrated that this matrix can be written as:

$$S_x = S_{smoothing} + S_{meas} + Sfwd.mod \tag{8}$$

From Eq.8, the smoothing error covariance matrix $S_{smoothing}$ represents the vertical sensitivity of the measurements to the retrieved profile:

$$S_{smoothing} = (A - I)S_a(A - I)^T \tag{9}$$

$S_{meas.}$ gives the contribution of the measurement error covariance matrix through S_m which illustrates the measured signal error covariance matrix, to the posterior error covariance matrix S_x. S_m is computed from the spectral noise:

$$S_{meas.} = GS_mG^T \tag{10}$$

At last, $S_{fwd.mod.}$ gives the contribution of the posterior error covariance matrix through S_f the forward model error covariance matrix, which illustrates the imperfect knowledge of the non-retrieved model parameters:

$$S_{fwd.mod.} = GK_bS_b(GK_b)^T = GS_fG^T \tag{11}$$

with S_b representing the error covariance matrix of the non-retrieved parameters.

3.3 A priori information

The IC analysis uses simulated radiance spectra of CHRIS in the bands: BT, B1, B2 and B3. The CO_2 and CH_4 vertical concentrations of the a priori state vector x_a are based on a profile that follows the criteria described in Section 3.1 divided by 20 vertical levels, extending from the ground to 20 km height with 1 km step. In addition, the water vapor vertical profile and the temperature are included in the non-retrieved parameters and will be discussed in Section 3.3.3. The a priori values and their variabilities are summarized in Table 1 and will be described in the following section.

3.3.1 A priori error covariance matrix

In situ data or climatology can give us an evaluation of the a priori error covariance matrix S_a. Nevertheless, the correlation of the vertical layers is more expressed by the off-diagonal matrix elements. Since this study is dedicated to information coming from the measurement rather than climatology's or in situ observations, we will always assume S_a as a diagonal matrix with the ith diagonal element ($S_{a,ii}$) defined as:

$$S_{a,ii} = \sigma_{a,i}^2 \quad \text{with} \quad \sigma_{a,i} = x_{a,i}.\frac{p_{error}}{100} \tag{12}$$

where $\sigma_{a,i}$ stands for the standard deviation in the Gaussian statistics formalism. The subscript i represents the ith parameter of the state vector.
The CO_2 profile a priori error is estimated from Schmidt and Khedim (1991). The CH_4 a priori error is fixed to p_{error}=5% similar to the one used in Razavi et al. (2009) for the inversion of the data obtained from IASI.

https://doi.org/10.5194/amt-2019-391
Preprint. Discussion started: 5 November 2019

Atmospheric Measurement Techniques Discussions

State vector elements	T	H_2O	CO_2	CH_4
a priori values x_a		US standard		
A priori uncertainty (P_{error})	1 K	10%	1.3-8%	5%

Table 1: State vector parameters.

3.3.2 Measurement error covariance matrix

The measurement error covariance matrix is computed knowing the instrument performance and accuracy. The latter is related to the radiometric noise expressed by the SNR already discussed in Section 2.2.2. This error covariance matrix is assumed to be diagonal, and the ith diagonal element can be computed as follows:

$$S_{m,ii} = \sigma_{m,i}^2 \quad \text{with} \quad \sigma_{m,i} = \frac{y_i}{SNR}, \tag{13}$$

where $\sigma_{m,i}$ is the standard deviation of the ith measurement (y_i) of the measurement vector y, representing the noise equivalent spectral radiance. The SNR for CHRIS is found in Table 2.

3.3.3 Non-retrieved parameter characterization and accuracy

The effects of non-retrieved parameters is a complicated part of an error description model. In our case these uncertainties are limited to the interfering water vapor molecules due to its important existence in the spectra and the effect of the temperature, where a vertically uniform uncertainty is assumed in both cases.
On one hand, we assumed a partial column with an uncertainty (p_{Cmol}) of 10% instead of a profile error for H_2O. On the other hand, we assumed a realistic uncertainty of $\delta T = 1K$, compatible with the typical values used for the ECMWF assimilation, on each layer of the temperature profile.
The total forward model error covariance matrix (S_f), assumed diagonal in the present study, is given by summing the contributions of each diagonal element, and the ith diagonal element ($S_{f,ii}$) is given by:

$$S_{f,ii} = \sum_{j=1}^{nlevel} \sigma_{f,T_j,i}^2 + \sigma_{f,H_2O,i} \tag{14}$$

Here, the spectroscopic effects such as the line parameter, the line mixing and the continua errors are not considered.

3.4 Information content analysis applied to greenhouse gases profiles

An information content analysis is performed on the whole spectrum for CO_2 and CH_4 separately to quantify the benefit of the multispectral synergy. Separately means that the state vector is constituted of only one of the above gas concentrations at each level between 0 and 20 km. This corresponds to the case where we estimated each gas profile alone when all other atmospheric parameters and all other gas profiles are known from ancillary data with a specific variability or uncertainty. Two different SZA (10° and 80°) are chosen to demonstrate the effect of the solar optical path on the study since the sensitivity is correlated to the viewing geometry.
Figure 5 and 6 show the averaging kernel A and total posterior error S_x for CO_2 and CH_4 respectively for an angle of 10°. The same is done for 80° and is used only to compare with the results of the 10° angle. A is obtained for each greenhouse gas independently using the variability introduced in Section 3.3.1, and considering an observing system composed of the band BT, B1, B2 or B3 separately and all the bands together. Each colored line represents the row of A at each vertical grid layer. Each peak of A represents the partial degree of freedom of the gas at each level that indicates the proportion of the information provided by the measurement. In fact, if the value is close to unity, it means that the information comes predominantly from the measurement, but a value close to zero means that the information comes mainly from our prior knowledge of the system (a priori state).
For CO_2, for an angle of 10°, the total DOFS are 2.56, 2.42, 3.12 and 3.52 for the bands BT, B1, B3 and all bands respectively and for an angle of 80° the DOFS are 2.6, 2.74, 3.46 and 3.79 for the same bands. This parameter show that one might be able to retrieve between 3 and 4 partial tropospheric columns for CO_2, and as expected the DOFS is slightly higher at 80° since the optical path of the sun in every layer is longer. Fig.5 shows that the information about CO_2 arises from the ground to 12 km high

https://doi.org/10.5194/amt-2019-391
Preprint. Discussion started: 5 November 2019

Atmospheric Measurement Techniques Discussions

	Resolution (cm^{-1})	MOPD (cm)	Spectral region (cm^{-1})	SNR
CHRIS	0.135	4.42	BT: 680-1250 B1: 1800-2300 B2: 2400-3600 B3: 3900-5200	780
EM27-SUN	0.5	1.8	B3: 4700-5200 B4: 5460-7200 B5: 7370-12500	1080
IFS125HR	5x10^{-3}	45	5-50000	1000

Table 2: Instrumental characteristics of CHRIS, EM27-SUN and IFS125HR.

in the atmosphere, while at much higher altitudes the information comes mainly from the a priori, due to a smaller sensitivity to CO_2 in the upper troposphere. This is also shown in the error budget study: in the lower part of the atmosphere (between 0 and 12 km), the a posteriori total error (solid black line) is significantly smaller than the a priori error (red line), which means that the measurement improved our knowledge of the CO_2 profile; while beyond 12 km, the total a posteriori error is equal to the a priori error suggesting a very poor sensitivity at high altitudes. Also, the vertical information distribution is improved when all the bands are used simultaneously. Furthermore, one can notice that the measurement error stays very weak regardless of the band used which proves that our SNR is largely sufficient and does not limit the inversion process. Also, the forward model error depending on the non-retrieved parameters remains quite modest. However, the smoothing error predominates the other errors and becomes preponderant beyond 12 km, which means that the information is strongly constrained by the a priori profile at high altitudes, and little information is introduced from the measurement.

The same reasoning is presented for CH_4: for an angle of 10°, the total DOFS, for bands BT, 2, 3 and all bands respectively are: 3.16, 3.55, 2.82 and 3.86; and for an angle of 80° the DOFS for the same bands are: 3.28, 3.95, 3.53 and 4.27. These slightly better values show that retrieving tropospheric columns for CH_4 from such measurements is as efficient as CO_2. Fig.6 shows that the vertical distribution of CH_4 is more homogeneous than that of CO_2 and we can see that the A's are broader than those of CO_2, suggesting a very important correlation between layers. The forward model error is systematically weaker than the measurement error, unlike CO_2, due to the fact that the methane bands are less impacted by the interfering molecules, especially H_2O (see Fig. 4).

As a general result, the simultaneous use of all the bands instead of using each one separately increases the total DOFS and reduces systematically the total errors of the two species. Finally, the total profile error is derived from the relative values of the diagonal matrix of S_x. The CO_2 total profile error for CHRIS is estimated to be 2.62%, whereas the CH_4 total profile error is 4.22%. Clearly, these results show that the total profile error for CH_4 is almost 2 times higher than that of CO_2, but this is explained by the fact that our profile error is limited by the a priori profile error which is much higher for CH_4 than for CO_2.

3.5 Comparison and complementary information content analysis for HR125, EM27 and CHRIS

During the MAGIC campaigns, several EM27-SUN and one IFS125HR were operated alongside CHRIS showed in Fig. 7. An extensive information content analysis is presented in the following sections for both of these instruments in order to compare and complement the study performed on CHRIS in Section 3.4.

3.5.1 Complementary information with EM27-SUN

In this section, an extensive IC study is presented for the EM27-SUN instrument in order to compare it with our results and to investigate the possibility of complementing the data we obtained from CHRIS. The bands of EM27 used in this study are denoted as follows: B3, the common band with CHRIS, with a spectral range of 4700-5200 cm^{-1}, B4 going from 5460 cm^{-1} to 7200 cm^{-1}, and B5 spanning the spectral region between 7370 and 12500 cm^{-1}.

Firstly, an information content study is performed on EM27-SUN for CO_2 and CH_4 separately. As mentioned in Section 3.4, the state vector is constituted of only one of the gases concentrations with the same profile at a layer going from 0 to 20 Km; however, we took into account the SNR and spectral resolution specific to this instrument (see Table 2). Table 3 shows the

https://doi.org/10.5194/amt-2019-391
Preprint. Discussion started: 5 November 2019

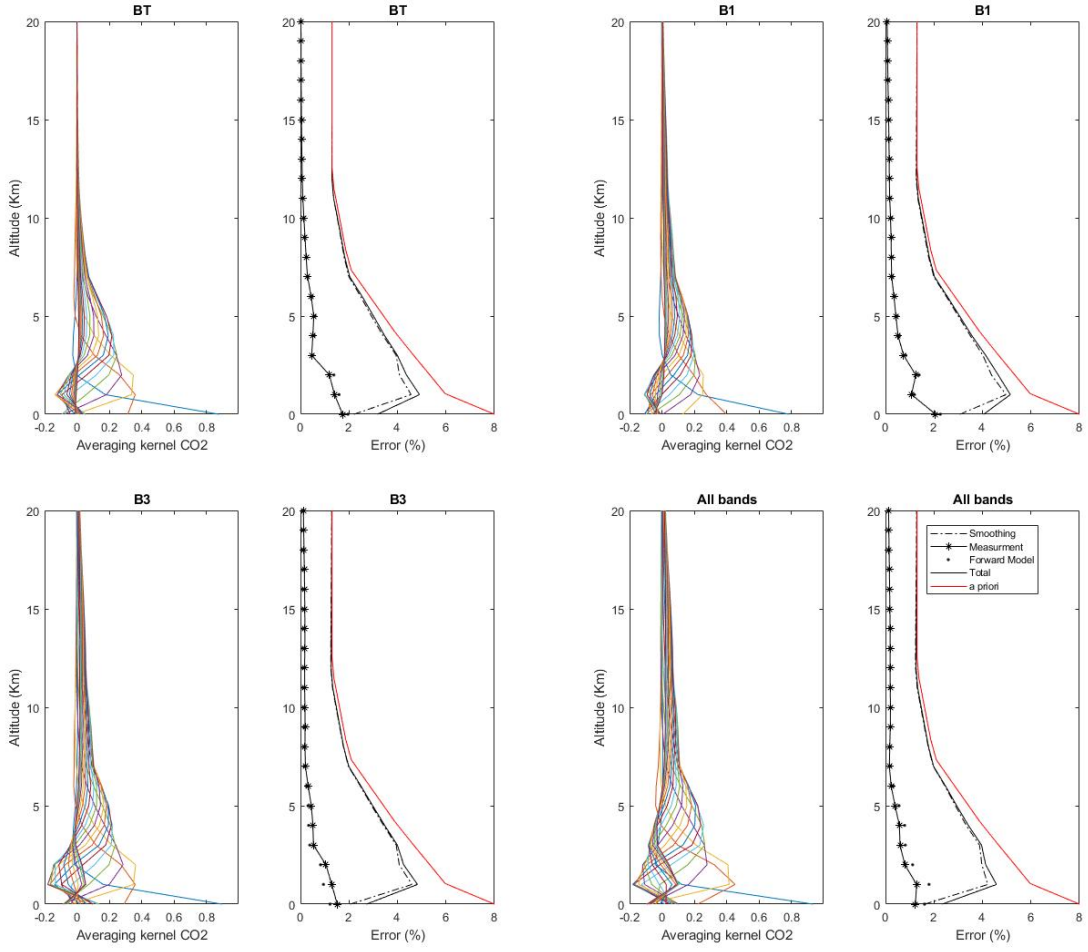

Fig. 5: Averaging kernels and error budgets of CO_2 vertical profiles for bands BT, B1 and B3 separately and all the bands together for an angle of 10° for CHRIS. The red and solid black lines stand for the prior (S_a) and posterior (S_x) errors respectively; the smoothing ($S_{smoothing}$), measurement ($S_{meas.}$), and forward model parameters ($S_{fwd.mod.}$) errors are dashed/dotted, dashed/starred and dotted, respectively.

DOFS for CO_2 of EM27-SUN: for an angle of 10°, the total DOFS for bands B3 (common band with CHRIS), B4 and all bands together are: 2.98, 1.65 and 3.06 respectively, compared to 3.2, 2.36 and 3.34 for an angle of 80°. If only band B3 is taken into consideration which is the common band between the two instruments, the DOFS of CHRIS in this band is, as stated before, 3.12 and 3.46 for an angle of 10° and 80° respectively, compared to 2.98 and 3.2 for EM27. Therefore, the same number of columns can be retrieved using CHRIS (see Section 3.4) for CO_2 in this band. However, an additional column can be retrieved using CHRIS if all the bands are used. Similar to the reasoning for CHRIS followed in Section 3.4, this study shows that using all the EM27-SUN bands together leads to an improvement of the a posteriori error profile on CO_2 concentrations, especially in the lower part of the atmosphere. As for CH_4 and referring to Table 2, band 3 in this instrument begins (4700 cm^{-1}) where the CH_4 band ends (4150-4700 cm^{-1}) in IFS125HR and CHRIS. This is important because TCCON networks often begin their measurements at 4700 cm^{-1} to coincide with the EM27-SUN and satellite data, therefore eliminating the CH_4 band from their spectra, this is why CHRIS and EM27-SUN have no common methane bands so the results will not be discussed here.
Secondly, a simultaneous IC study was performed on all the channels of both CHRIS and EM27-SUN in order to analyze

https://doi.org/10.5194/amt-2019-391
Preprint. Discussion started: 5 November 2019

Atmospheric Measurement Techniques Discussions

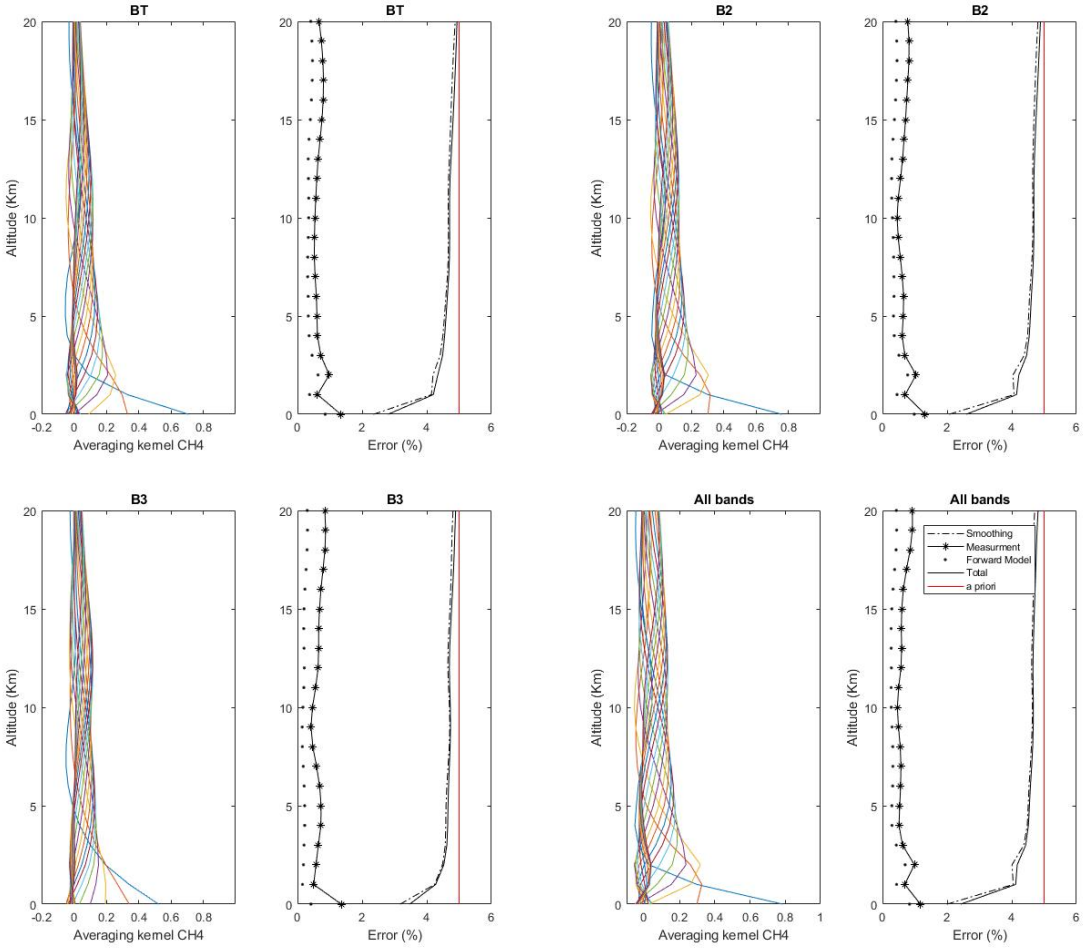

Fig. 6: Same as Fig. 5, but for CH_4 with bands BT, B2, B3 and all the bands together.

Fig. 7: The CHRIS spectrometer with the attached tracker during one the 2018 MAGIC campaigns.

https://doi.org/10.5194/amt-2019-391
Preprint. Discussion started: 5 November 2019

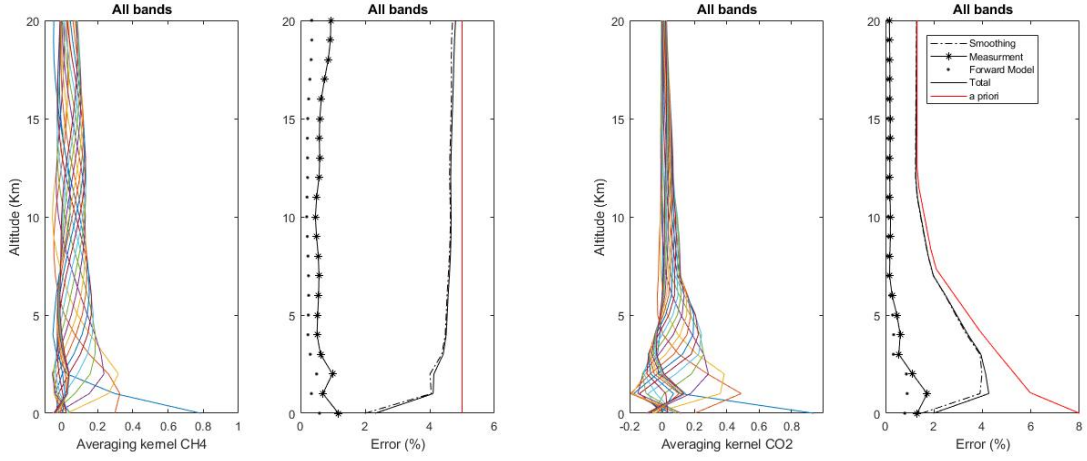

Fig. 8: Averaging kernels and error budgets of CO_2 and CH_4 vertical profiles for all the bands together for EM27 and CHRIS combined for an angle of 10°. The red and black lines stand for the prior (S_a) and posterior (S_x) errors respectively; the smoothing ($S_{smoothing}$), measurement ($S_{meas.}$), and forward model parameters ($S_{fwd.mod.}$) errors are dashed/dotted, dashed/starred and dotted, respectively.

		BT	B1	B3	B4	All bands	
		DOFS				DOFS	Error
CHRIS	Angle 10	2.56	2.42	3.12	-	3.52	2.62%
	Angle 80	2.6	2.74	3.46	-	3.79	2.55%
EM27-SUN	Angle 10	-	-	2.98	1.65	3.06	2.74%
	Angle 80	-	-	3.2	2.36	3.34	2.64%
IFS125HR	Angle 10	2.89	2.86	3.72	2.73	4.32	2.54%
	Angle 80	2.91	3.25	4.07	3.22	4.56	2.48%

Table 3: The DOFS and column errors (%) of CO_2 for each band and for each instrument.

the complementary aspect of these two instruments. The results of this study are shown in Fig. 8. The DOFS obtained for CO_2 is 3.58 and 3.9 for angles 10° and 80° respectively; and for CH_4 3.87 and 4.29. This indicates a slight improvement in the retrieval, but less than the one obtained from space (for example TANSO-FTS in Herbin et al. (2013a)) where the coupling TIR/SWIR, gives an advantage over the more pronounced difference MIR/SWIR between CHRIS and EM27-SUN. In addition, the computational time is very large, so the benefit of a simultaneous retrieval depends on the additional computing time generated.

However, in the NIR, the error budget is performed by monitoring the observed O_2 columns where column-averaged dry-air mole fractions (denoted X_G for gas G) is calculated by rationing the gas retrieved slant column to the O_2 retrieved slant column for the same spectrum, which allows the reduction of a major part of the bias and the systematic errors during the measurement and its inversion process. The calculation of X_G will allow the EM27-SUN community to compare their results with the satellites data. This is not possible for CHRIS because it covers the MIR region where the O_2 molecule is missing in the spectra.

https://doi.org/10.5194/amt-2019-391
Preprint. Discussion started: 5 November 2019

Atmospheric Measurement Techniques Discussions

		BT	B2	B3	B4	All bands	
		DOFS				DOFS	Error
CHRIS	Angle 10	3.16	3.55	2.82	-	3.86	4.22%
	Angle 80	3.28	3.95	3.53	-	4.27	4.13%
EM27-SUN	Angle 10	-	-	-	1.73	1.73	4.67%
	Angle 80	-	-	-	2.47	2.47	4.51%
IFS125HR	Angle 10	3.93	4.51	3.87	2.69	4.88	4.09%
	Angle 80	4.11	4.88	4.41	3.51	5.27	3.98%

Table 4: The DOFS and column errors (%) of CH_4 for each band and for each instrument.

3.5.2 Comparison with IFS125HR

As mentioned before, IFS125HR is a ground-based high resolution infrared spectrometer installed in many of the NDACC stations, and some TCCON stations with a SNR of the order of 1000 (Schneider and Hase (2008)). We performed an information content study on this instrument to compare it with our results. For simplicity, the same annotation of the bands is kept for this section. The same methodology described in Section 3.4 is used here: the state vector is constituted of only CO_2 and CH_4 concentrations at a layer going from 0 to 20 km where the SNR and the spectral resolution specific to the IFS125HR instrument are taken into consideration.

We follow the same reasoning as the sections before: the DOFS of CO_2, as shown in Table 3, for an angle of 10° are: 2.89, 2.86, 3.72, 2.73 and 4.32 for BT, B1, B3, B4 and all bands respectively, compared to 2.91, 3.25, 4.07, 3.22 and 4.56 for an angle of 80°. However, the DOFS of CH_4 , as shown in Table 4, for an angle of 10° are: 3.93, 4.51, 3.87, 2.69 and 4.88 for BT, B2, B3, B4 and all bands respectively, compared to 4.11, 4.88, 4.41, 3.51 and 5.27 for an angle of 80°. On the one hand, one additional partial tropospheric column for CO_2 can be retrieved with respect to: CHRIS for an angle of 80°, and EM27-SUN for both angles, if all the bands are used. We obtain the same result for CH_4, one additional partial tropospheric column can be retrieved with respect to CHRIS, if B3 or all the bands are used and for both angles. However, three additional partial tropospheric columns can be retrieved with respect to the EM27-SUN instrument.

Figure 9 shows the averaging kernel A and the total posterior error S_x for CO_2 and CH_4, for an angle of 10°. As a first look, we can see that the vertical distribution is more homogeneous than CHRIS and EM27-SUN suggesting a high sensitivity at high altitudes although in the lower atmosphere, the a posteriori error S_x is significantly reduced. This is also shown in the error budget study: we can still distinguish the a posteriori total error (solid black line) from the a priori error (red line) even in the higher atmosphere. This is explained by the fact that the IFS125HR has a spectral resolution 30 times higher than CHRIS and 100 times higher than EM27-SUN, so the measurement will always improve our knowledge of the profile all along the atmospheric column. This result, along with the one discussed in Section 3.5.1, shows that CHRIS is more efficient than the EM27-SUN and less efficient than the IFS125HR in terms of the retrieval of GHG measurements.

	CO_2		CH_4	
DOFS	90%	99%	90%	99%
Number of channels	1329	4648	1387	5924
% of the total number of channels	2.15%	7.54%	2.25%	9.61%

Table 5: Corresponding number of selected channels for the DOFS of CO_2 and CH_4 and their respective percentage of the total number of channels for CHRIS.

https://doi.org/10.5194/amt-2019-391
Preprint. Discussion started: 5 November 2019

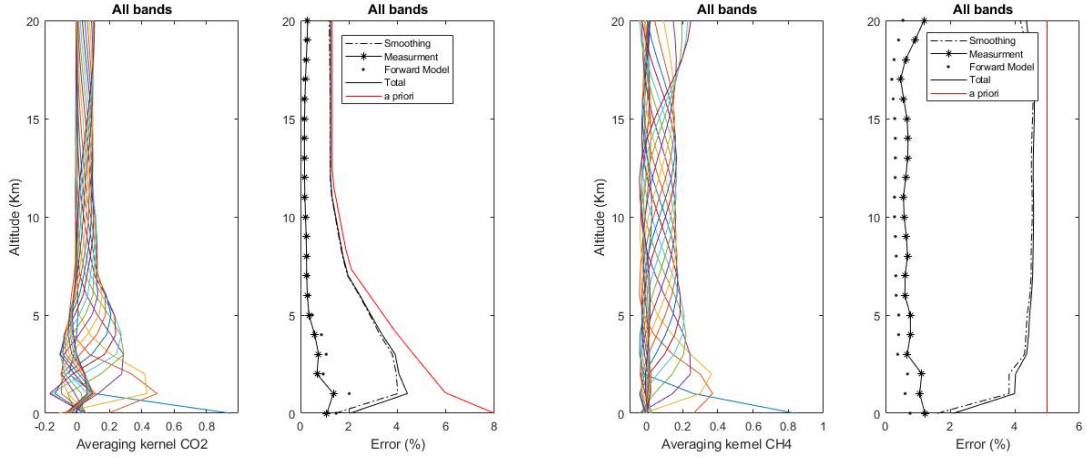

Fig. 9: Averaging kernels and error budgets of CO_2 and CH_4 and vertical profiles for bands all the bands together for an angle of 10° for IFS125HR. The red and black lines stand for the prior (S_a) and posterior (S_x) errors respectively; the smoothing ($S_{smoothing}$), measurement ($S_{meas.}$), and forward model parameters ($S_{fwd.mod.}$) errors are dashed/dotted, dashed/starred and dotted, respectively.

4 Channel selection

Using all the channels, measured by CHRIS, in the retrieval scheme has two disadvantages. First of all, it requires a very large computational time. Secondly, the correlation of the interfering species increases the systematic error. In this case, the a priori state vector x_a and the error covariance matrix S_a is very difficult to evaluate. Channel selection is a method described by Rodgers (2000) to optimize a retrieval by objectively selecting the subset of channels that provides the greatest amount of information from high-resolution infrared sounders. L'Ecuyer et al. (2006) offers a description of this procedure based on the Shannon information content. This approach is based on a sequential modification of the covariance matrix that will reduce the amount of time needed to perform the numerous matrix operations necessary for repeated application of the previous equations. Firstly, we create what we call an "information spectrum" in order to evaluate the information content with respect to the a priori state vector. The channel with the largest amount of information is then selected. A new spectrum is then calculated with a new posterior covariance matrix that is adjusted according to the channel selected on the first iteration to account for the information it provides. In this way a second channel is chosen, based on this newly defined state space, that provides maximal information relative to the new a posterior covariance matrix. This process is repeated and channels are selected sequentially until the information in all the remaining channels falls below the level of measurement noise. As stated by Shannon information content and noted in Rodgers (2000), it is convenient to work in a basis where the measurement errors and prior variances are uncorrelated in order to compare the measurement error with the natural variability of the measurements across the full prior state. Therefore, it is desirable to transform K into $\widetilde{K}$ using:

$$\widetilde{K} = S_y^{-1/2} K S_a^{1/2} \tag{15}$$

which offers the added benefit of being the basis where both the a priori and the measurement covariance matrices are unit matrices. Furthermore, Rodgers demonstrates that the number of singular values of $\widetilde{K}$ greater than unity defines the number of independent measurements that exceed the measurement noise defining the effective rank of the problem.
Letting S_i be the error covariance matrix for the state space after i channels have been selected, the information content of channel j of the remaining unselected channels is given by:

$$H_j = \frac{1}{2} log_2(1 + \widetilde{k}_j^T S_i \widetilde{k}_j), \tag{16}$$

https://doi.org/10.5194/amt-2019-391
Preprint. Discussion started: 5 November 2019

Atmospheric Measurement Techniques Discussions

where $\widetilde{k}_j$ is the jth row of $\widetilde{K}$. H_j constitutes the information spectrum from which the first channel is selected. Taking the chosen channel to be channel l, the covariance matrix is then updated before the next iteration using the following statement:

$$S_{i+1}^{-1} = S_i^{-1} + \widetilde{k}_l \widetilde{k}_l^T \tag{17}$$

In this way, channels are selected until 90% of the total information spectrum H is reached in a way that the measurement noise is not exceeded.

After that H expressed in bits is converted to DOFS to obtain Fig. 10 that represents the CO_2 and CH_4 total DOFS evolution as a function of the number of selected channels and from all spectral bands and for a SZA of 10°. CHRIS has 75424 channels in total, 13800 are unusable because of the water vapor saturation between the bands, which leaves us with 61624 exploitable channels. A pre-selection of these channels, based on Fig.4, is done where the number of exploitable channels is reduced to the spectral areas where we find CO_2 and CH_4 . At a first look at Figure 10, the DOFS for each gas increases sharply with the first selected channels and then more steadily. The number of channels required to reach 90% and 99% of the total information provided by using all the channels is represented in Table 5. For CO_2, out of the 1329 channels, 55.76% of the information comes from B3 (common band with the EM27), 37.24% from BT and 6.99% from B1. As for CH_4, out of the 1387 channels, 46.86% of the information comes from B2, 28.19% from BT and 24.9% from B3. This result shows that most of the information for CO_2 and CH_4 comes from band 3 (B3) and the thermal band (BT) respectively, which indicates that the synergy between TIR and SWIR observations is confirmed.

Furthermore, the 1329 and 1387 selected channels represent 2.15% and 2.25% of the 61624 exploitable channels respectively, so a retrieval scheme that uses selected channels corresponding to 90% of the total information content would give comparable errors to the one using the entire set of channels since almost 98% of the information is redundant. Hence, these results indicate the interest of determining an optimal set of channels for each gas separately, so the inversion process will be easier and less time consuming.

5 Conclusions

To summarize, the work done in this paper, presents the characteristics of a new infrared spectrometer called CHRIS that allows the retrieval of GHG and trace gases. In the context of its exploitation in field campaigns, especially MAGIC, to retrieve GHG, we calibrated this instrument spectrally and radiometrically as well as performed an extensive information content analysis. A comparison and a complementary study was made, for two commercial ground-based instruments, one of them being part of the TCCON network.The possibility of a retrieval exploiting the synergy between TIR and SWIR observations was also discussed. Future work will focus on the retrieval of tropospheric columns and the inversion process of the GHG, CO_2 and CH_4, using the line-by-line radiative transfer algorithm ARAHMIS and the validation of our results with the MAGIC campaign data.

Acknowledgements. The CaPPA project (Chemical and Physical Properties of the Atmosphere) is funded by the French National Research Agency (ANR) through the PIA (Programme d'Investissement d'Avenir) under contract "ANR-11-LABX-0005-01" and by the Regional Council "Nord Pas de Calais-Picardie" and the "European Funds for Regional Economic Development" (FEDER). Financial support from CNES TOSCA (MAGIC) is also acknowledged.

Also we acknowledge the "Ecole centrale de lille" for its help in providing the cavity blackbody used in the calibration process. IT support from Fabrice Ducos is also acknowledged.

References

Aumann, H. H., Chahine, M. T., Gautier, C., Goldberg, M. D., Kalnay, E., McMillin L. M., Revercomb, H., Rosenkranz, P. W., Smith, W. L., Staelin, D. H., Strow, L. L., and Susskind, J.: *AIRS/AMSU/HSB on the Aqua mission: design, science objectives, data products, and processing systems*, IEEE Trans. Geosci. Remote Sens., 41, 253-264, https://doi.org/10.1109/TGRS.2002.808356, 2003.

Clarisse, L., Hurtmans, D., Prata, A. J., Karagulian, F., Clerbaux, C., Mazière, M. D., and Coheur, P.-F.: Retrieving radius, concentration, optical depth, and mass of different types of aerosols from high-resolution infrared nadir spectra, Appl. Opt., 49, 3713-3722, 10.1364/AO.49.003713, 2010.

Clerbaux, C., Hadji-Lazaro, J., Turquety, S., George, M., Coheur, P.-F., Hurtmans, D., Wespes, C., Herbin, H., Blumstein, D., Tourniers, B., and Phulpin, T.: The IASI/MetOp1 Mission: First observations and highlights of its potential contribution to GMES2, Space Res. Today, 168, 19-24, https://doi.org/10.1016/S0045-8732(07)80046-5, 2007.

Gisi, M., Hase, F., Dohe, S., Blumenstock, T., Simon, A., and Keens, A.: XCO_2-measurements with a tabletop FTS using solar absorption spectroscopy, Atmos. Meas. Tech., 5, 2969-2980, https://doi.org/10.5194/amt-5-2969-2012, 2012.

https://doi.org/10.5194/amt-2019-391
Preprint. Discussion started: 5 November 2019

Atmospheric Measurement Techniques Discussions

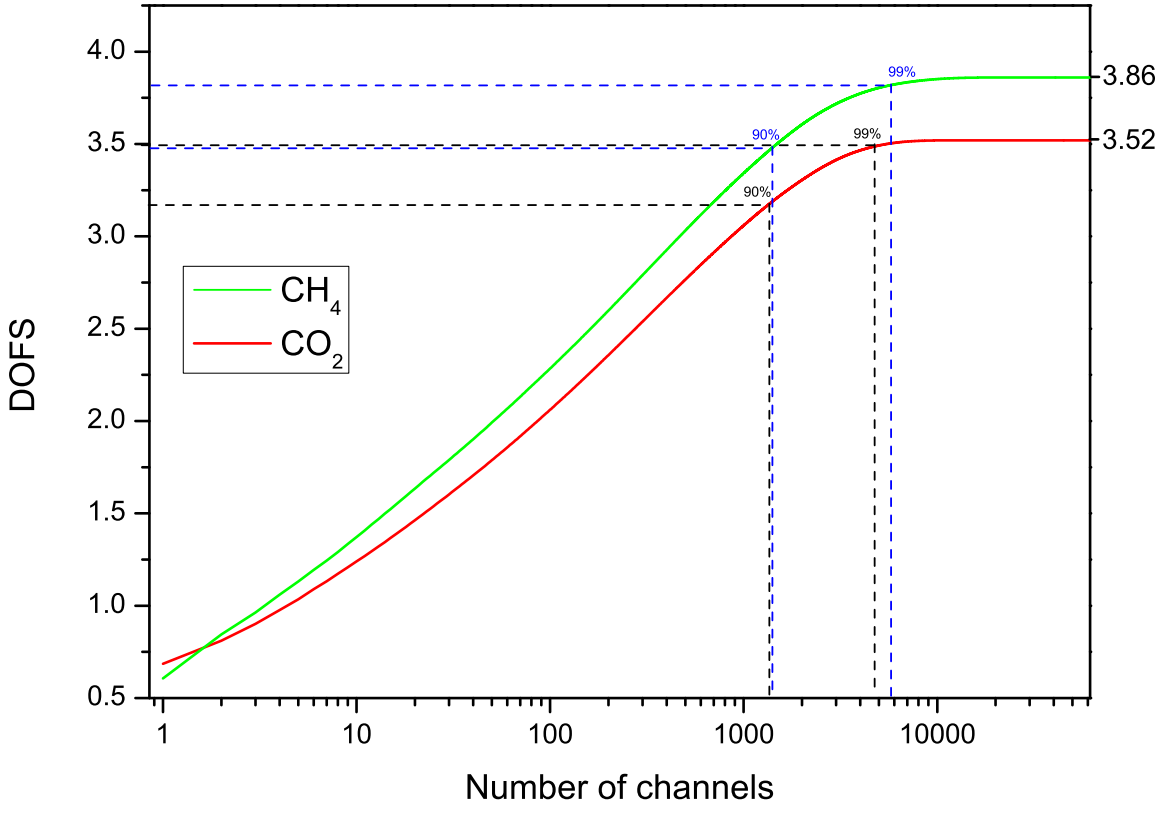

Fig. 10: Evolution of the DOFSs with the number of selected channels for CO_2 (red line) and CO_2 (green line).

Gordon, I. E., Rothman, L. S., Hill, C., Kochanov, R. V., Tan, Y., Bernath, P. F., Birk, M., Boudon, V., Campargue, A., Chance, K., Drouin, B. J., Flaud, J.-M., Gamache, R. R., Hodges, J. T., Jacquemart, D., Perevalov, V. I., Perrin, A., Shine, K. P., Smith, M.-A. H., Tennyson, J., Toon, G. C., Tran, H., Tyuterev, V. G., Barbe, A., Császár, A. G., Devi, V. M., Furtenbacher, T., Harrison, J. J., Hartmann, J.-M., Jolly, A., Johnson, T. J., Karman, T., Kleiner, I., Kyuberis, A. A., Loos, J., Lyulin, O. M., Massie, S. T., Mikhailenko, S. N., Moazzen-Ahmadi, N., Muller, H. S. P., Naumenko, O. V., Nikitin, A. V., Polyansky, O. L., Rey, M., Rotger, M., Sharpe, S. W., Sung, K., Starikova, E., Tashkun, S. A., Auwera, J. V., Wagner, G., Wilzewski, J., Wcislo, P., Yu, S., and Zak, E.J.: The HITRAN2016 molecular spectroscopic database, J. Quant. Spectrosc. Radiat. Transf., 203, 3-69, https://doi.org/10.1016/j.jqsrt.2017.06.038, 2017.

Herbin, H., Labonnote, L. C., and Dubuisson, P.: Multispectral information from TANSO-FTS instrument – Part 1: Application to greenhouse gases (CO_2 and CH_4) in clear sky conditions, Atmos. Meas. Tech., 6, 3301–3311, https://doi.org/10.5194/amt-6-3301-2013, 2013.

Kobayashi, N., Inoue, G., Kawasaki, M., Yoshioka, H., Minomura, M., Murata, I., Nagahama, T., Matsumi, Y., Tanaka, T., Morino, I., and Ibuki, T.: Remotely operable compact instruments for measuring atmospheric CO_2 and CH_4 column densities at surface monitoring sites, Atmos. Meas. Tech., 3, 1103–1112, https://doi.org/10.5194/amt-3-1103-2010, 2010.

L'Ecuyer, T. S., Gabriel, P., Leesman, K., Cooper, S. J., Stephens, G. L.: Objective Assessment of the Information Content of Visible and Infrared Radiance Measurements for Cloud Microphysical Property Retrievals over the Global Oceans. Part I: Liquid Clouds, J. Appl. Meteorol. Clim., 45, 20-41, https://doi.org/10.1175/JAM2326.1, 2006.

Michalsky, J. J.: The Astronomical Almanac's algorithm for approximate solar position (1950–2050), J. Sol. Energy, 40, 227-235, https://doi.org/10.1016/0038-092X(88)90045-X, 1988.

Pathakoti, M., Gaddamidi, S., Gharai, B., Mullapudi Venkata Rama, S. S., Kumar Sundaran, R., and Wang, W.: Retrieval of CO_2, CH_4, CO and N_2O using ground- based FTIR data and validation against satellite observations over the Shadnagar, India, Atmos. Meas. Tech. Discuss., https://doi.org/10.5194/amt-2019-7, 2019.

Persky, M. J.: A review of spaceborne infrared Fourier transform spectrometers for remote sensing, Rev. Sci. Instrum., 66, 4763-4797, https://doi.org/10.1063/1.1146154, 1995.

https://doi.org/10.5194/amt-2019-391
Preprint. Discussion started: 5 November 2019

Atmospheric Measurement Techniques Discussions

Petri, C., Warneke, T., Jones, N., Ridder, T., Messerschmidt, J., Weinzierl, T., Geibel, M., and Notholt, J.: Remote sensing of CO_2 and CH_4 using solar absorption spectrometry with a low resolution spectrometer, Atmos. Meas. Tech., 5, 1627–1635, https://doi.org/10.5194/amt-5-1627-2012, 2012.

Razavi, A., Clerbaux, C., Wespes, C., Clarisse, L., Hurtmans, D., Payan, S., Camy-Peyret, C., and Coheur, P. F.: Characterization of methane retrievals from the IASI space-borne sounder, Atmos. Chem. Phys., 9, 7889-7899, https://doi.org/10.5194/acp-9-7889-2009, 2009.

Revercomb, H. E., Buijs, H., Howell, H. B., LaPorte, D. D., Smith, W. L., and Sromovsky, L. A.: Radiometric calibration of IR Fourier transform spectrometers: solution to a problem with the High-Resolution Interferometer Sounder, Appl. Opt., 27, 3210-3218, https://doi.org/10.1364/AO.27.003210, 1988.

Rodgers, C. D.: Inverse methods for atmospheric sounding : theory and practice, World Scientific Publishing, 2000.

Schmidt, U., and Khedim, A.: In situ measurements of carbon dioxide in the winter Arctic vortex and at midlatitudes : an indicator of the age of stratopheric air, Geophys. Res. Lett., 18, 763-766, https://doi.org/10.1029/91GL00022, 1991.

Schneider, M. and Hase, F.: Technical Note: Recipe for monitoring of total ozone with a precision of around 1 DU applying mid-infrared solar absorption spectra, Atmos. Chem. Phys., 8, 63-71, https://doi.org/10.5194/acp-8-63-2008, 2008.

Suto, H., Kuze, A., Kaneko, Y., and Hamazaki, T.: Characterization of TANSO-FTS on GOSAT, AGU Fall Meeting Abstracts, 2006.

Toon, G. C., Solar Line List for the TCCON 2014 Data Release, CaltechDATA, https://doi.org/10.14291/tccon.ggg2014.solar.r0/1221658, 2015.

Trishchenko, A. P.: Solar Irradiance and Effective Brightness Temperature for SWIR Channels of AVHRR/NOAA and GOES Imagers, J. Atmospheric Ocean. Technol., 23, 198-210, https://doi.org/10.1175/JTECH1850.1, 2006.

Wunch, D., Toon, G. C., Blavier, J.-F. L., Washenfelder, R. A., Notholt, J., Connor, B. J., Griffith, D. W. T., Sherlock, V., and Wennberg, P. O.: The Total Carbon Column Observing Network, Philos. Trans. Royal Soc. A, 369, 2087-2112, https://doi.org/10.1098/rsta.2010.0240, 2011.